

Electromagnetically induced transparency and nonlinear pulse propagation in an atomic medium confined in a waveguide

Liang Li,¹ Chengjie Zhu,¹ L. Deng,² and Guoxiang Huang^{1,*}

¹State Key Laboratory of Precision Spectroscopy and Department of Physics, East China Normal University, Shanghai 200062, China

²Physics Laboratory, National Institute of Standards and Technology, Gaithersburg, Maryland 20899, USA

*Corresponding author: gxhuang@phy.ecnu.edu.cn

Received August 22, 2012; revised October 31, 2012; accepted November 24, 2012;
posted November 26, 2012 (Doc. ID 174785); published December 19, 2012

We study electromagnetically induced transparency (EIT) and nonlinear pulse propagation in a resonant atomic gas confined in a microwaveguide. We find that the quantum-interference effect in this system can be greatly enhanced due to the reduction of the mode volume of the optical field. In particular, compared with atomic gases in free space, the EIT transparency window in the present confined system can be much wider and deeper, the group velocity of the probe field can be much slower, and the Kerr nonlinearity of the system can be much stronger. We show that a more efficient production of ultraslow optical solitons in the present system may be achieved with much slower propagating velocity and lower generation power. Features of EIT and pulse propagation in the present system are very promising for practical applications in optical information processing and transmission. © 2012 Optical Society of America

OCIS codes: 020.1670, 230.7390, 270.5530.

1. INTRODUCTION

In recent years, optical wave propagation in coherent media has attracted much attention due to the finding of electromagnetically induced transparency (EIT) [1]. It has been shown that EIT can be used not only for suppression of optical absorption but also for reduction of group velocity and enhancement of Kerr nonlinearity, and so on [2]. These features of EIT may lead to many applications, such as slow light [3], quantum memory [4], highly entangled photons [5], quantum phase gates [6,7], efficient multiwave mixing [8–10], weak-light ultraslow solitons [11,12], and optical clocks [13].

Because of their sharp energy levels and excellent quantum coherence, atomic gaseous phase media are very attractive candidates for high-precision manipulation of single quantum states. For practical applications, solid-state setups have the advantages of scalability and integrability, benefiting directly from the development of micro- and nanotechnologies. Compared with gaseous phase media, however, solid-state media usually have large decoherence, a challenging problem for quantum information processing at single quantum level. One of methods to solve this problem is to use quantum hybrid systems, which can combine the advantages of atomic gases and solid-state elements via a quantum interface in compatible experimental setups [14].

Most previous works on EIT have been performed with bulk atomic samples. Recently, there have been some efforts made on EIT study in gaseous phase media confined in microstructures, such as hollow-core photonic-crystal fibers [15,16], antiresonant reflecting optical waveguides [17], and nanofibers [18], etc. However, confinement-enhanced quantum-interference effect and EIT-related, ultraslow temporal optical

soliton propagation in such confined systems have not been reported up to now.

In this article, we investigate the quantum-interference effect and nonlinear pulse propagation in a resonant atomic gas confined in a microwaveguide. We find that EIT effect in this confined system can be greatly enhanced due to the reduction of the mode volume of optical field. Particularly, in comparison with atomic gases in free space, the EIT transparency window in the present system is much wider and deeper, the group velocity of the probe field is much slower, and the Kerr nonlinearity of the system is much stronger. We find also that an efficient production of ultraslow optical solitons in the present confined system may be achieved with much slower propagating velocity and lower generation power than that needed in unconfined systems adopted in [11,12]. Novel features of EIT and pulse propagation in the present system are very promising for practical applications in optical information processing and transmission. We note that in [19,20], solitonlike nonlinear pulse propagations in gas-filled hollow-core photonic-crystal fibers are studied [19,20]. However, in these studies, no resonant interaction between the optical field and atoms and the EIT are considered. In [21] and [22], spatial solitons in a planar hollow-core waveguide and in arrayed and checkerboard optical waveguides via EIT are studied respectively, but no confinement-enhanced quantum-interference effect and ultraslow temporal optical solitons are considered.

The paper is arranged as follows. Section 2 describes our waveguide model. Section 3 studies the linear propagation of the probe field and analyzes the EIT characters of the system in detail. In Section 4, a weak-nonlinear perturbation theory is employed to study the nonlinear pulse

propagation. Finally, Section 5 summarizes the main results of our work.

2. MODEL

We consider an atomic gas that is filled in the space between two identical, parallel perfect metal plates with separation L , which is the order of magnitude of optical wave length; see Fig. 1(a). The lower plate of the structure is chosen as the $z = 0$ plane of the coordinate system shown in Fig. 1(b). We assume that the linear dimension of the metal plates is much larger than L and consider the light propagation in this waveguide system.

Electric field vector $\mathbf{E} \equiv (E_x, E_y, E_z)$ in the absence of the atomic gas can be obtained by solving Maxwell equations under the boundary conditions $E_x = E_y = 0$ and $\partial E_z / \partial z = 0$ on the surfaces $z = 0$ and L , which in general consist of many different dispersion branches, with dispersion relations $\omega_n \equiv \omega_n(\mathbf{k}_{\parallel}) = c\sqrt{\mathbf{k}_{\parallel}^2 + n^2\pi^2/L^2}$ ($n = 0, 1, 2, \dots$). Assuming the modes excited in the waveguide belong to the TE component with a given mode index n , one has $\mathbf{E}^{\text{TE}}(\mathbf{r}, t) = \sum_{k_x, k_y} \left(\frac{\hbar\omega_n}{\epsilon_0 V}\right)^{1/2} a_n^{\text{TE}} \sin\left(\frac{n\pi z}{L}\right) (\hat{\mathbf{k}}_{\parallel} \times \mathbf{e}_z) e^{i\theta_n} + \text{h.c.}$ Here $V = SL$ is the mode volume (S is the area of the plates), $\theta_n \equiv \mathbf{k}_{\parallel} \cdot \mathbf{r} - \omega_n t$, $\mathbf{k}_{\parallel} \equiv (k_x, k_y, 0)$, $\hat{\mathbf{k}}_{\parallel} \equiv \mathbf{k}_{\parallel}/|\mathbf{k}_{\parallel}|$, $\mathbf{e}_z = (0, 0, 1)$, and h.c. represents Hermitian conjugate. In the quantized form of the optical field, a_n^{TE} is the annihilation operator of photons.

Note that k_x and k_y can take any continuous values but n is a nonnegative integer, which means that the optical field can propagate in the xy -plane but is confined between the two plates of the waveguide. Choosing the optical field being polarized in the x -direction and propagating in the y -direction, we have

$$\mathbf{E}^{\text{TE}}(\mathbf{r}, t) = \mathbf{e}_x \sum_k \mathcal{E}_k \sin\left(\frac{n\pi z}{L}\right) \exp[i(ky - \bar{\omega}t)] + \text{h.c.}, \quad (1)$$

where $k \equiv k_y$, $\bar{\omega} \equiv \omega_n(k) = c[k^2 + (n\pi/L)^2]^{1/2}$, and $\mathcal{E}_k \equiv (\hbar\bar{\omega}/\epsilon_0 V)^{1/2} a_n^{\text{TE}}(k)$. We see that the optical field is

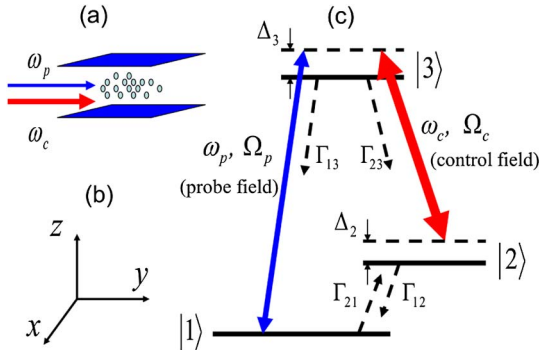


Fig. 1. (Color online) (a) Waveguide consisting of two parallel perfect metal plates and filled with the atomic gas. (b) Specified coordinate system. (c) Energy-level diagram and excitation scheme of three-level Λ system, in which a weak (strong) probe (control) field of central angular frequency ω_p (ω_c) and half Rabi frequency Ω_p (Ω_c) couples to the atomic states $|1\rangle$, $|2\rangle$, and $|3\rangle$. Γ_{13} and Γ_{23} are spontaneous-emission decay rates from $|3\rangle$ to $|1\rangle$ and $|3\rangle$ to $|2\rangle$, respectively; Γ_{12} and Γ_{21} denote incoherent population exchange between $|1\rangle$ and $|2\rangle$. Δ_2 and Δ_3 are two- and one-photon detunings, respectively.

inversely proportional to \sqrt{V} ; thus it is enhanced if L becomes small.

For convenience, we take k as a function of ω . Then Eq. (1) can be expressed as

$$\mathbf{E}(\mathbf{r}, t) = \mathbf{e}_x \sum_{\bar{\omega}} \mathcal{E}_{\bar{\omega}} \sin\left(\frac{n\pi z}{L}\right) \exp\{i[k(\bar{\omega})y - \bar{\omega}t]\} + \text{h.c.} \quad (2)$$

with

$$k(\bar{\omega}) = \left[\left(\frac{\bar{\omega}}{c}\right)^2 - \left(\frac{n\pi}{L}\right)^2 \right]^{1/2}. \quad (3)$$

To excite a wave mode with the given index n , the frequency $\bar{\omega}$ must be large than $n\pi c/L$. Notice that in Eq. (2) the symbol “TE” has been omitted.

We assume the filled atoms have three-level configuration [Fig. 1(c)], where two lower states $|1\rangle$ and $|2\rangle$ belong to the same ground-state hyperfine manifold whereas state $|3\rangle$ is an excited state. A weak (strong) probe (control) field of central angular frequency ω_p (ω_c) is injected in the y -direction [see Fig. 1(a)]. The probe field couples to the $|1\rangle \leftrightarrow |3\rangle$ transition and the control field couples the $|2\rangle \leftrightarrow |3\rangle$ transition. One- and two-photon detunings are respectively $\Delta_3 = \omega_p - (\omega_3 - \omega_1)$ and $\Delta_2 = \omega_p - \omega_c - (\omega_2 - \omega_1)$, with $\hbar\omega_j$ being the eigen energy of the state $|j\rangle$. Γ_{13} and Γ_{23} represent the spontaneous decay rate from $|3\rangle$ to $|1\rangle$ and $|3\rangle$ to $|2\rangle$, respectively. The hyperfine ground states $|1\rangle$ and $|2\rangle$ are electric dipole forbidden, but between them there is an incoherent population exchange with rates Γ_{12} and Γ_{21} , describing the transit-time effect due to the entering and leaving of atoms in the interaction region.

Assume the probe and control fields are the modes belonging to those given by Eq. (2). The existence of atoms will modulate the electric-field envelope; i.e., \mathcal{E} becomes a function of x , y , and t . Thus Eq. (2) is changed into

$$\mathbf{E}(\mathbf{r}, t) = \mathbf{e}_x \sum_{l=p,c} \mathcal{E}_l(x, y, t) \sin\left(\frac{n\pi z}{L}\right) \exp[i(k_l y - \omega_l t)] + \text{h.c.} \quad (4)$$

with $k_l \equiv k(\omega_l)$ ($l = p, c$) [23].

Under electric-dipole and rotating-wave approximations, the Hamiltonian of the system in interaction picture is given by

$$\hat{\mathcal{H}}_I = -\hbar[\zeta(z)\Omega_p^* e^{-ik_p y - \omega_p t} |1\rangle\langle 3| + \zeta(z)\Omega_c^* e^{-ik_c y - \omega_c t} |2\rangle\langle 3|] + \text{h.c.}, \quad (5)$$

where $\zeta(z) \equiv \sin(n\pi/L)z$ is the mode function in the z -direction, and $\Omega_p \equiv (\mathbf{e}_x \cdot \mathbf{p}_{31})\mathcal{E}_p/\hbar$ ($\Omega_c \equiv (\mathbf{e}_x \cdot \mathbf{p}_{32})\mathcal{E}_c/\hbar$) is the half Rabi frequency of the probe (control) field, with $\mathbf{p}_{jl} \equiv \langle j|\mathbf{p}|l\rangle$. The equations of motion of the density matrix $\tilde{\sigma}$ in the interaction picture are

$$i\frac{\partial}{\partial t} \tilde{\sigma}_{11} + i\Gamma_{21} \tilde{\sigma}_{11} - i\Gamma_{12} \tilde{\sigma}_{22} - i\Gamma_{13} \tilde{\sigma}_{33} + \zeta^*(z)\Omega_p^* \tilde{\sigma}_{31} - \zeta(z)\Omega_p \tilde{\sigma}_{31}^* = 0, \quad (6a)$$

$$i\frac{\partial}{\partial t} \tilde{\sigma}_{22} - i\Gamma_{21} \tilde{\sigma}_{11} + i\Gamma_{12} \tilde{\sigma}_{22} - i\Gamma_{23} \tilde{\sigma}_{33} + \zeta^*(z)\Omega_c^* \tilde{\sigma}_{32} - \zeta(z)\Omega_c \tilde{\sigma}_{32}^* = 0, \quad (6b)$$

$$i \frac{\partial}{\partial t} \tilde{\sigma}_{33} + i \Gamma_3 \tilde{\sigma}_{33} - \zeta^*(z) \Omega_p^* \tilde{\sigma}_{31} + \zeta(z) \Omega_p \tilde{\sigma}_{31}^* - \zeta^*(z) \Omega_c^* \tilde{\sigma}_{32} + \zeta(z) \Omega_c \tilde{\sigma}_{32}^* = 0, \quad (6c)$$

$$\left(i \frac{\partial}{\partial t} + d_{21} \right) \tilde{\sigma}_{21} - \zeta(z) \Omega_p \tilde{\sigma}_{32}^* + \zeta^*(z) \Omega_c^* \tilde{\sigma}_{31} = 0, \quad (6d)$$

$$\left(i \frac{\partial}{\partial t} + d_{31} \right) \tilde{\sigma}_{31} - \zeta(z) \Omega_p (\tilde{\sigma}_{33} - \tilde{\sigma}_{11}) + \zeta(z) \Omega_c \tilde{\sigma}_{21} = 0, \quad (6e)$$

$$\left(i \frac{\partial}{\partial t} + d_{32} \right) \tilde{\sigma}_{32} - \zeta(z) \Omega_c (\tilde{\sigma}_{33} - \tilde{\sigma}_{22}) + \zeta(z) \Omega_p \tilde{\sigma}_{21}^* = 0 \quad (6f)$$

with $d_{jl} = \Delta_j - \Delta_l + i\gamma_{jl}$. Here $\gamma_{jl} = (1/2)(\Gamma_j + \Gamma_l) + \gamma_{jl}^{\text{col}}$, with $\Gamma_1 = \Gamma_{21}$, $\Gamma_2 = \Gamma_{12}$, $\Gamma_3 = \Gamma_{13} + \Gamma_{23}$, and γ_{jl}^{col} are the dephasing rates caused by collisions.

In the semiclassical framework, the propagation of electromagnetic waves is described by the Maxwell equation for the electric field

$$\nabla^2 \mathbf{E} - \frac{1}{c^2} \frac{\partial^2 \mathbf{E}}{\partial t^2} = \frac{1}{\epsilon_0 c^2} \frac{\partial^2 \mathbf{P}}{\partial t^2},$$

where $\mathbf{P} = \mathcal{N}_\alpha (\mathbf{p}_{31} \sigma_{13} e^{i(k_y y - \omega_p t)} + \mathbf{p}_{32} \sigma_{23} e^{i(k_y y - \omega_c t)} + \text{c.c.})$ is the electric polarization with \mathcal{N}_α being the density of atoms. Using the expression (4) and slow-varying envelope approximation, we obtain

$$\zeta(z) \left[i \left(n_{\text{WG}} \frac{\partial}{\partial y} + \frac{1}{c} \frac{\partial}{\partial t} \right) + \frac{c}{2\omega_p} \frac{\partial^2}{\partial x^2} \right] \Omega_p(x, y, t) + \kappa_{13} \tilde{\sigma}_{31}(z; x, y, t) = 0.$$

Note that in deriving the above equation we have assumed higher-order eigenmodes of the waveguide are not excited. This is reasonable approximation because the present waveguide is a highly confined system with its higher-order eigenmodes having large excitation energy. The peak power (see below) of the optical pulse we consider is small and hence the excitation of the higher-order eigenmodes can be neglected. In the above equation, (x, y, t) are slow variables. Multiplying $\zeta^*(z)$ and making the integration from 0 to L on the fast variable z , one obtains

$$\left[i \left(n_{\text{WG}} \frac{\partial}{\partial y} + \frac{1}{c} \frac{\partial}{\partial t} \right) + \frac{c}{2\omega_p} \frac{\partial^2}{\partial x^2} \right] \Omega_p(x, y, t) + \kappa_{13} \langle \tilde{\sigma}_{31}(z; x, y, t) \rangle = 0, \quad (7)$$

where $\kappa_{13} = \mathcal{N}_\alpha \omega_p |\mathbf{p}_{13}|^2 / (2\epsilon_0 c \hbar)$,

$$n_{\text{WG}} \equiv \frac{k(\omega_p) c}{\omega_p} = \left[1 - \left(\frac{c}{\omega_p} \frac{n\pi}{L} \right)^2 \right]^{1/2} \quad (8)$$

is the effective refraction index of the waveguide in the absence of atoms, and $\langle f(z) \rangle \equiv \int_0^L dz \zeta^*(z) f(z) / \int_0^L dz |\zeta(z)|^2$.

Notice that compared with three-level atoms in free space, there are several interesting features for the present waveguide system, which are reflected in the Maxwell-Bloch

(MB) Eqs. (6) and (7): (i) the mode function of the waveguide in the z -direction, i.e., $\zeta(z)$, appears in the Bloch Eq. (6); (ii) the effective refraction index of the waveguide, i.e., n_{WG} , appears in the Maxwell Eq. (7). In particular, from the last term on the left-hand side of Eq. (7) we see that the confinement effect may result in a significant increase of the interaction between the atoms and the optical field because n_{WG} can be much less than 1.

3. EIT CHARACTERS IN THE WAVEGUIDE SYSTEM

A. Base State

To analyze EIT characters in the waveguide system and study nonlinear pulse propagation (see the next section), one should know the base state of the MB Eqs. (6) and (7). The base state is the steady state of the MB equations when the probe field is absent (i.e., $\partial/\partial t = 0$, $\Omega_p = 0$). It is easy to obtain such a state as

$$\tilde{\sigma}_{11}^{(0)} = \frac{X_1 \Gamma_{12} \Gamma_3 + \Gamma_{12} |\zeta(z) \Omega_c|^2 + \Gamma_{13} |\zeta(z) \Omega_c|^2}{X_2}, \quad (9a)$$

$$\tilde{\sigma}_{22}^{(0)} = \frac{X_1 \Gamma_{21} \Gamma_3 + \Gamma_{21} |\zeta(z) \Omega_c|^2}{X_2}, \quad (9b)$$

$$\tilde{\sigma}_{33}^{(0)} = \frac{\Gamma_{21} |\zeta(z) \Omega_c|^2}{X_2}, \quad (9c)$$

$$\tilde{\sigma}_{32}^{(0)} = -\frac{\zeta(z) \Omega_c X_1 \Gamma_{21} \Gamma_3}{d_{32} X_2}, \quad (9d)$$

and $\tilde{\sigma}_{21}^{(0)} = \tilde{\sigma}_{31}^{(0)} = 0$, where $X_1 = [(\Delta_3 - \Delta_2)^2 + \Gamma_{32}^2] / (2\Gamma_{32})$ and $X_2 = X_1 (\Gamma_{21} + \Gamma_{12}) \Gamma_3 + (2\Gamma_{21} + \Gamma_{12}) |\zeta(z) \Omega_c|^2 + \Gamma_{13} |\zeta(z) \Omega_c|^2$.

We see that due to the existence of the incoherent population exchange from $|1\rangle$ to $|2\rangle$ (i.e., $\Gamma_{21} \neq 0$), there is population distributed in the states $|2\rangle$ and $|3\rangle$. Note that different from the conventional situation (i.e., $\Gamma_{21} = 0$) [2], we have a non-vanishing $\tilde{\sigma}_{32}^{(0)}$. It should be pointed out that such coherence is due to the existence of the control field. The role of the incoherent population exchange is only to provide a passage of the atoms from $|1\rangle$ to $|2\rangle$. Through the control field, the population in $|2\rangle$ is transferred into $|3\rangle$. As a result, a Raman-like gain will appear for the probe field [see Eq. (11) below].

B. EIT Characters

The linear excitation of the system can be obtained by linearizing the Eq. (6) around the based state (9). The solving process is the same as that in [12]. Assuming the beamwidth of the probe pulse in the x -direction is large enough (e.g., unfocused beam), one can disregard the diffraction term in Eq. (7). Then by taking Ω_p and $\tilde{\sigma}_{j1}$ ($j = 2, 3$) as small quantities proportional to $\exp(i\theta)$ with $\theta = K(\omega)y - \omega t$, we obtain the linear dispersion relation of the system

$$K(\omega) = \frac{\omega}{cn_{\text{WG}}} + \frac{\kappa_{13}}{n_{\text{WG}}} \left\langle \frac{(\omega + d_{21})(2\tilde{\sigma}_{11}^{(0)} + \tilde{\sigma}_{22}^{(0)} - 1) + \zeta(z)\Omega_c\tilde{\sigma}_{32}^{*(0)}}{|\zeta(z)\Omega_c|^2 - (\omega + d_{21})(\omega + d_{31})} \right\rangle. \quad (10)$$

By Taylor expanding $K(\omega)$ as $K(\omega) = K_0 + K_1\omega + (1/2)K_2\omega^2 + (1/6)K_3\omega^3 + \dots$, we obtain the dispersion coefficients in different orders, given by $K_j = [\partial^j K(\omega)/\partial \omega^j]_{\omega=0}$.

The imaginary part of $K(\omega)$ evaluated at the center frequency of the probe field (corresponding to $\omega = 0$) for $\Delta_2 = \Delta_3 = 0$ reads

$$\text{Im}(K_0) = \frac{\kappa_{13}}{n_{\text{WG}}} \left\langle \frac{\gamma_{21}}{|\zeta(z)\Omega_c|^2 + \gamma_{21}\Gamma_{31}} - \frac{\Gamma_{21}}{|\zeta(z)\Omega_c|^2 + 2\gamma_{21}\Gamma_{31}} \right\rangle. \quad (11)$$

The average in the second term on the right-hand side (RHS) of Eqs. (10) and (11) must be evaluated numerically.

Based on Eqs. (10) and (11), we have the following conclusions:

(1) The value of $\text{Im}(K)$ is not only a function of ω , but also is strongly L -dependent. Shown in Fig. 2 is the probe-field absorption profile $\text{Im}(K)$ as a function of ω and L . The dot-dashed, dashed, and solid curves are for $L = 4.0, 2.0,$ and $1.0 \mu\text{m}$, respectively. From the figure we see that (i) an EIT transparency window is opened, which is due to the quantum-interference effect induced by the control field; (ii) the EIT transparency window can be enlarged significantly by decreasing L . The smaller the L , the larger the EIT transparency window. The EIT transparency window for $L = 1 \mu\text{m}$ is obviously much wider and deeper than that for $L = 4 \mu\text{m}$. Hence the confinement effect provided by the waveguide geometry can be used to obtain a more pronounced EIT effect compared with that in free space. Note that when plotting the figure, we have chosen the D_1 line transitions of the ^{87}Rb atoms with $|1\rangle = |5S_{1/2}, F=1\rangle$, $|2\rangle = |5S_{1/2}, F=2\rangle$, and $|3\rangle = |5P_{1/2}, F=1\rangle$. System parameters used here (and also in the following) are $\kappa_{13} = 1.0 \times 10^9 \text{ cm}^{-1} \text{ s}^{-1}$, $\gamma_{21} = 10^{-4}\gamma_{31}$.

(2) Using Eq. (10), we obtain the group velocity $v_g \equiv [\text{Re}(\partial K/\partial \omega)]^{-1}$ of the probe field. Shown in Fig. 3(a) is the

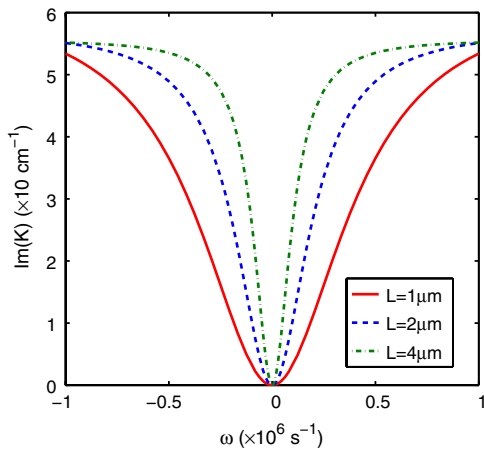


Fig. 2. (Color online) $\text{Im}(K)$ as a function of ω and L . The dot-dashed, dashed, and solid curves are for $L = 4.0, 2.0,$ and $1.0 \mu\text{m}$, respectively.

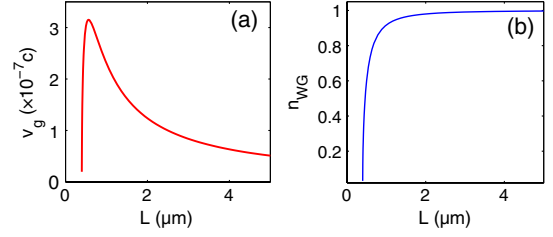


Fig. 3. (Color online) (a) Group velocity v_g as a function of L . (b) Effective refractive index n_{WG} of the waveguide as a function of L .

result of v_g as a function of L evaluated at $\omega = 0$. We see that at first v_g increases as L is reduced from a large value, then it arrives at maximum, and later it decreases rapidly as L is reduced to a small value. The reason is that the effective refractive index of the waveguide n_{WG} is very sensitive to the waveguide parameter L , as shown in Fig. 3(b). For a small L , the confinement is significant and the effective refractive index $n_{\text{WG}} \rightarrow 0$, which contributes to a extremely slow group velocity. On the other hand, for large L one has $n_{\text{WG}} \approx 1$, and hence v_g will not change greatly. In this case the system is equivalent to that in free space.

(3) The second term on the RHS of Eq. (11) contributes a gain induced by the incoherent population exchange (i.e., Γ_{21}), which can be used to reduce the absorption coming mainly from the dephasing γ_{21}^{col} since $\gamma_{21} \approx \gamma_{21}^{\text{col}}$. The physical reason for such gain is that Γ_{21} provides a passage of population from $|1\rangle$ to $|2\rangle$, and then to $|3\rangle$ through the action of the control field, resulting in the Raman-like gain for the probe field. The gain can also be suppressed greatly when $|\Omega_c|$ is large.

Shown in Fig. 4 is the result of $\text{Im}(K_0)$ as a function of $|\Omega_c|$. The solid (dashed) curve in the figure is for $\Gamma_{21} = 0$ ($\Gamma_{21} = \gamma_{21}$). We see that for small $|\Omega_c|$, $\text{Im}(K_0)$ is large, but when increasing $|\Omega_c|$, the value of $\text{Im}(K_0)$ decreases rapidly. In addition, the incoherent population exchange (i.e., $\Gamma_{21} \neq 0$) can also be used to suppress the absorption, and hence the dashed curve is lower than the solid curve. The inset in the figure shows the result of the function “ratio”/100, where “ratio” $\equiv \text{Im}(K_0)_{\Gamma_{21}=0}/\text{Im}(K_0)_{\Gamma_{21}=\gamma_{21}}$, which indicates that $\text{Im}(K_0)_{\Gamma_{21}=\gamma_{21}}$ is only 1/200 of $\text{Im}(K_0)_{\Gamma_{21}=0}$ for $\Omega_c = 1.0 \times 10^6 \text{ s}^{-1}$.

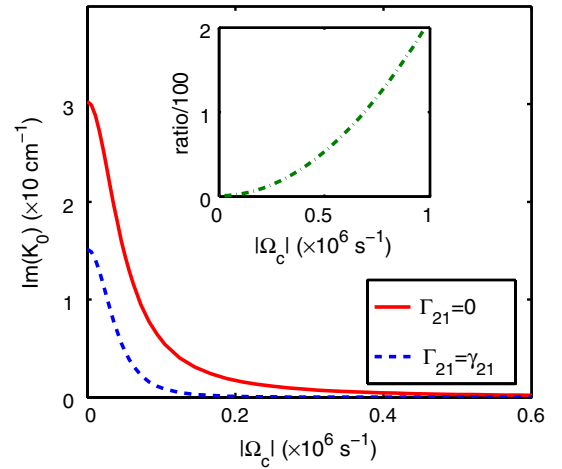


Fig. 4. (Color online) $\text{Im}(K_0)$ as a function of $|\Omega_c|$ with $\Gamma_{21} = 0$ (solid curve) and $\Gamma_{21} = \gamma_{21}$ (dashed curve). The inset shows the result of the function “ratio”/100, where “ratio” $\equiv \text{Im}(K_0)_{\Gamma_{21}=0}/\text{Im}(K_0)_{\Gamma_{21}=\gamma_{21}}$.

4. NONLINEAR PULSE PROPAGATION

One pronounced effect associated with the optical pulse propagation in a waveguide system, such as optical fiber, is the significant increase of power density and suppression of diffraction in confined directions. In telecommunications, even a low power injected into a waveguide can generate sizable signals via an optical four-wave mixing process, which necessarily requires a high local power density. Correspondingly, it is easier to form optical solitons in an optical waveguide, which also requires a significant power density to produce a sizable local nonlinearity to balance the dispersion effect. Thus, the high power density of confined atomic systems must also be considered in the configuration studied here. This is of practical interest for applications in optical information processing and transmission in quantum hybrid systems when shape-preserving probe pulse propagation with a low pump power is needed.

A. Nonlinear Envelope Equation

A standard technique for studying weak nonlinear effects in dispersive systems is the method of multiple scales [12]. We take the expansion $\tilde{\sigma}_{jl} = \tilde{\sigma}_{jl}^{(0)} + \epsilon \tilde{\sigma}_{jl}^{(1)} + \epsilon^2 \tilde{\sigma}_{jl}^{(2)} + \epsilon^3 \tilde{\sigma}_{jl}^{(3)} + \dots$, $\Omega_p = \epsilon \Omega_p^{(1)} + \epsilon^2 \Omega_p^{(2)} + \epsilon^3 \Omega_p^{(3)} + \dots$, where ϵ is a small parameter characterizing the typical amplitude of the probe field and $\tilde{\sigma}_{jl}^{(0)}$ is the base-state solution given by Eq. (9). To obtain a divergence-free expansion, all quantities on the RHS of the expansion are considered as functions of the multiscale variables $y_m = \epsilon^m y$ ($m = 0, 1, 2$), and $t_m = \epsilon^m t$ ($m = 0, 1$). Substituting these expansions into Eqs. (6) and (7), one obtains a series of equations for $\tilde{\sigma}_{ij}^{(l)}$ and $\Omega_p^{(l)}$ ($l = 1, 2, 3, \dots$), which can be solved order by order.

At the leading order, we obtain

$$\Omega_p^{(1)} = F e^{i\theta}, \quad (12a)$$

$$\tilde{\sigma}_{31}^{(1)} = \frac{(\omega + d_{21})(2\tilde{\sigma}_{11}^{(0)} + \tilde{\sigma}_{22}^{(0)} - 1) + \zeta(z)\Omega_c \tilde{\sigma}_{32}^{(0)}}{|\zeta(z)\Omega_c|^2 - (\omega + d_{21})(\omega + \bar{d}_{31})} F e^{i\theta}, \quad (12b)$$

$$\tilde{\sigma}_{21}^{(1)} = -\frac{(\omega + \bar{d}_{31})\tilde{\sigma}_{32}^{*(0)} + \zeta(z)\Omega_c^*(2\tilde{\sigma}_{11}^{(0)} + \tilde{\sigma}_{22}^{(0)} - 1)}{|\zeta(z)\Omega_c|^2 - (\omega + d_{21})(\omega + \bar{d}_{31})} F e^{i\theta} \quad (12b)$$

with other $\tilde{\sigma}_{jl}^{(1)} = 0$. Here $\theta = K(\omega)y_0 - \omega t_0$ and F is a yet-to-be-determined envelope function. The linear dispersion relation $K(\omega)$ has been given in Eq. (10).

At the second order, a divergence-free solution for $\Omega_p^{(2)}$ requires $i[\partial F/\partial y_1 + (1/v_g)\partial F/\partial t_1] = 0$. The second-order solutions, $\tilde{\sigma}_{11}^{(2)}$, $\tilde{\sigma}_{22}^{(2)}$, and $\tilde{\sigma}_{32}^{(2)}$, are given by

$$\tilde{\sigma}_{22}^{(2)} = \frac{-i}{\Gamma_{13} - \Gamma_{12}} \left\{ \left[\frac{(\omega + d_{21}^*)(2\sigma_{11}^{(0)} + \sigma_{22}^{(0)} - 1) + \zeta(z)\Omega_c^* \sigma_{32}^{(0)}}{|\zeta(z)\Omega_c|^2 - (\omega + d_{21})(\omega + d_{31})} - \text{c.c.} \right] - i(\Gamma_{21} + \Gamma_{13})a_{11}^{(2)} \right\}, \quad (13b)$$

$$\tilde{\sigma}_{32}^{(2)} = \frac{1}{d_{32}} \left[\frac{\zeta(z)(\omega + d_{31}^*)\sigma_{32}^{(0)} + \Omega_c(2\sigma_{11}^{(0)} + \sigma_{22}^{(0)} - 1)}{|\zeta(z)\Omega_c|^2 - (\omega + d_{21}^*)(\omega + d_{31}^*)} - \Omega_c(a_{11}^{(2)} + 2a_{22}^{(2)}) \right]. \quad (13c)$$

At the third order, substituting Eq. (13) into Eq. (7), we obtain the nonlinear envelope equation for F :

$$i \frac{\partial F}{\partial y_2} + \frac{c}{2\omega_p n_{\text{WG}}} \frac{\partial^2}{\partial x_1^2} F - \frac{1}{2} \frac{\partial^2 K}{\partial \omega^2} \frac{\partial^2 F}{\partial t_1^2} - W|F|^2 F e^{-2i\bar{\alpha}y_2} = 0 \quad (14)$$

with

$$W = -\frac{\kappa_{13}}{n_{\text{WG}}} \left\langle \frac{1}{\zeta(z)} \frac{\zeta(z)\Omega_c \tilde{\sigma}_{32}^{*(2)} + (\omega + d_{21})(2\tilde{\sigma}_{11}^{(2)} + \tilde{\sigma}_{22}^{(2)})}{|\zeta(z)\Omega_c|^2 - (\omega + d_{21})(\omega + \bar{d}_{31})} \right\rangle \quad (15)$$

and $\bar{\alpha} = \epsilon^{-2} \text{Im}(K_0)$. The nonlinear coefficient W given in Eq. (15) is due to the Kerr effect, which results in a self-phase modulation of the probe field and its value is complex generally. In our model, the imaginary part of W is much less than its real part (see the example given below).

We stress that the confinement effect by the waveguide geometry can enhance the Kerr effect significantly. Illustrated in Fig. 5(a) is $\text{Re}(W)$ as a function of Δ_3 , evaluated at $\omega = 0$. The dashed and solid curves in the figure are for $L = 0.6$ and $0.4 \mu\text{m}$, respectively. We see that the Kerr effect for the case of large confinement ($L = 0.4 \mu\text{m}$) is much larger than that for the case of small confinement ($L = 0.6 \mu\text{m}$). Shown in the inset is the waveguide-size dependence of $\text{Re}(W)$ for $\Delta_3 = 1.0 \times 10^7 \text{ s}^{-1}$.

Shown in Fig. 5(b) is also $\text{Re}(W)$ as a function of Δ_3 evaluated at $\omega = 0$, but the dashed and solid curves in panel (b) are for $L = 4.0$ and $1.0 \mu\text{m}$, respectively. When plotting this figure, we have adjusted the control-field intensity to make the dispersion length $L_D \text{equiv} \tau_0^2/|K_2|$ in the two cases are approximately the same (see the inset of this figure). We see again that $\text{Re}(W)$ for the large confinement ($L = 1.0 \mu\text{m}$) is much larger than that for the small confinement ($L = 4.0 \mu\text{m}$).

$$\tilde{\sigma}_{11}^{(2)} = \left\{ \left[i(\Gamma_{12} + \Gamma_{23}) + 2|\zeta(z)\Omega_c|^2 \left(\frac{1}{d_{32}^*} - \frac{1}{d_{32}} \right) \right] \left[\frac{(\omega + d_{21}^*)(2\sigma_{11}^{(0)} + \sigma_{22}^{(0)} - 1) + \zeta(z)\Omega_c^* \sigma_{32}^{(0)}}{|\zeta(z)\Omega_c|^2 - (\omega + d_{21}^*)(\omega + d_{31}^*)} - \text{c.c.} \right] - i(\Gamma_{13} - \Gamma_{12}) \left[\frac{\zeta(z)\Omega_c \zeta(z)(\omega + d_{31})\sigma_{32}^{*(0)} + \Omega_c^*(2\sigma_{11}^{(0)} + \sigma_{22}^{(0)} - 1)}{d_{32}^*} - \text{c.c.} \right] \right\} / \left[i|\zeta(z)\Omega_c|^2 (2\Gamma_{21} + \Gamma_{12} + \Gamma_{13}) \left(\frac{1}{d_{32}^*} - \frac{1}{d_{32}} \right) - \Gamma_3(\Gamma_{12} + \Gamma_{21}) \right], \quad (13a)$$

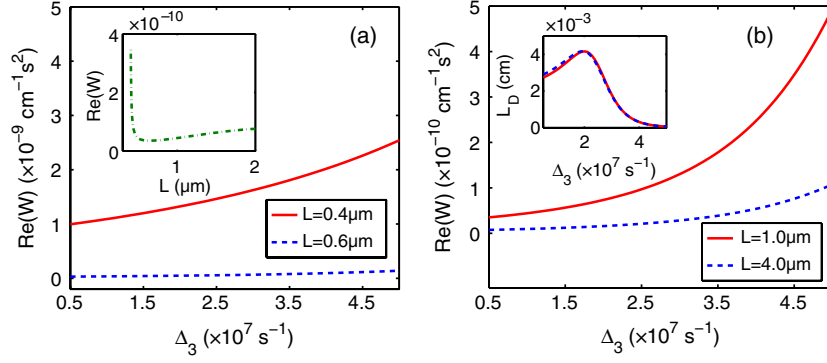


Fig. 5. (Color online) Nonlinear coefficient $\text{Re}(W)$ as a function of Δ_3 evaluated at $\omega = 0$. The dashed and solid curves in panel (a) are for $L = 0.6$ and $0.4 \mu\text{m}$, respectively. The inset shows the profile of $\text{Re}(W)$ as a function of L with $\Delta_3 = 1.0 \times 10^7 \text{ s}^{-1}$. The dashed and solid curves in panel (b) are for $L = 4.0$ and $1.0 \mu\text{m}$, respectively. The inset shows the corresponding dispersion length L_D for the two cases.

B. Ultraslow Solitons at Low-Light Level

When returning to original variables, Eq. (14) becomes

$$i\left(\frac{\partial}{\partial y} + \alpha\right)U + \frac{c}{2\omega_p n_{\text{WG}}} \frac{\partial^2 U}{\partial x^2} - \frac{1}{2} \frac{\partial^2 K}{\partial \omega^2} \frac{\partial^2 U}{\partial \tau^2} - W|U|^2 U e^{-2\alpha y} = 0, \quad (16)$$

where $\tau = t - y/v_g$ and $U = \epsilon F \exp(-i\alpha y)$. Near the center frequency of the probe field (i.e., $\omega = 0$), Eq. (16) can be written into the dimensionless form

$$i \frac{\partial u}{\partial s} + \frac{\partial^2 u}{\partial \sigma^2} + 2|u|^2 u = id_0 u + d_1 \frac{\partial^2 u}{\partial \eta^2} \quad (17)$$

with $s = -y/(2L_D)$, $\sigma = \tau/\tau_0$, $\eta = x/R_x$, and $u = U/U_0$. Here R_x is typical beam radius in x -direction, and $U_0 = (1/\tau_0)\sqrt{|K_2|/|W|}$ is typical Rabi frequency of the probe field. Dimensionless coefficients on the RHS of Eq. (17) are defined by $d_0 = L_D/L_A$ and $d_1 = L_D/L_{\text{diff}}$, with $L_A = 1/(2\alpha)$ being typical absorption length and $L_{\text{diff}} = \omega_p n_{\text{WG}} R_x^2/c$ being typical diffraction length.

If $d_0 \ll 1$ and $d_1 \ll 1$, Eq. (17) reduces to a standard nonlinear Schrödinger equation, which is completely integrable and allows multisoliton solutions. A single bright soliton solution reads $u = 2 \text{sech}[2\beta(\sigma - \sigma_0 + 4\delta s)] \exp[-2i\delta\sigma - 4i(\delta^2 - \beta^2)s - i\phi_0]$, where β , δ , σ_0 , and ϕ_0 are arbitrary real parameters. Taking $\beta = 1/2$ and $\delta = \sigma_0 = \phi_0 = 0$, we have $u = \text{sech} \sigma \exp(is)$. Then we have

$$\Omega_p = \frac{1}{\tau_0} \sqrt{\frac{|K_2|}{|W|}} \text{sech}\left[\frac{1}{\tau_0}\left(t - \frac{y}{v_g}\right)\right] \exp\left\{i\left[\text{Re}(K_0)y + \frac{y}{2L_D}\right]\right\}, \quad (18)$$

which describes a bright soliton traveling with propagating velocity v_g .

We now give a practical numerical example for the formation of the optical soliton given above. We choose ^{87}Rb D_1 -line transitions, with the system parameters given by $\kappa_{13} = 1.0 \times 10^9 \text{ cm}^{-1} \text{ s}^{-1}$, $\Omega_c = 3.0 \times 10^6 \text{ s}^{-1}$, $\Delta_2 = 2.1 \times 10^4 \text{ s}^{-1}$, $\Delta_3 = 5 \times 10^7 \text{ s}^{-1}$, and $L = 1.0 \mu\text{m}$. In this case, one has $K_2 = (2.15 + 0.83i) \times 10^{-11} \text{ cm}^{-1} \text{ s}^2$ and $W = (14.72 + 0.94i) \times 10^{-14} \text{ cm}^{-1} \text{ s}^2$. We see that the imaginary part of these coefficients is indeed much smaller than their real part, originated

from the quantum destructive interference effect induced by the control field. When taking $\tau_0 = 5.0 \times 10^{-6} \text{ s}$, $R_x = 0.05 \text{ cm}$, we have the characteristic lengths $L_D = 1.16 \text{ cm}$, $L_A = 40.67 \text{ cm}$, and $L_{\text{diff}} = 193.14 \text{ cm}$, which ensure the validity of the condition $d_0 \ll 1$ and $d_1 \ll 1$.

Using the above data it is easy to estimate the propagating velocity of the soliton, which reads

$$v_g = 2.62 \times 10^{-7} c. \quad (19)$$

Consequently, the optical soliton obtained in the present confined atomic gas may travel with ultraslow propagating velocity, which is one order of magnitude slower than that in free-space EIT schemes [12].

The maximum input power for generating the ultraslow optical soliton can be estimated by calculating Poynting's vector. The density of average flux of energy over a carrier-wave period reads $P/S_0 = (P_{\text{max}}/S_0) \text{sech}^2[(t - z/v_g)/\tau_0]$. Here $S_0 = R_x L$ and P_{max} is the maximum input power. Shown in Fig. 6 is the density of maximum input power P_{max}/S_0 as a function of L . From the figure we see that the larger the confinement effect of the waveguide (i.e., the smaller L), the smaller the density of maximum input power P_{max}/S_0 . Using the above parameters, for $L = 1 \mu\text{m}$ we obtain

$$P_{\text{max}} = 2.5 \times 10^{-6} \text{ W}. \quad (20)$$

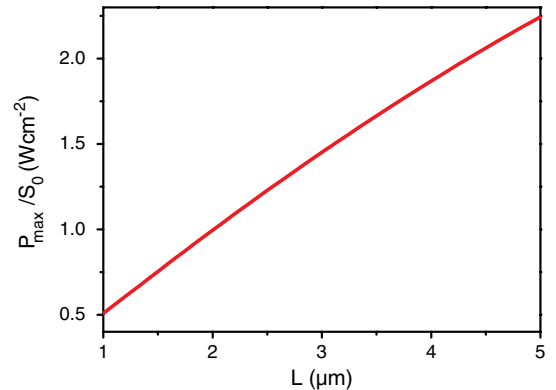


Fig. 6. (Color online) Density of maximum input power P_{max}/S_0 for producing the ultraslow optical soliton as a function of L .

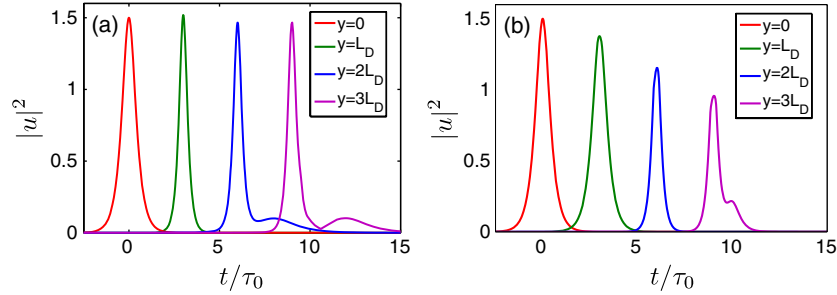


Fig. 7. (Color online) Evolution of the dimensionless probe-field intensity $|u|^2$ as a function of dimensionless time t/τ_0 . The curves from left to right are waveshapes after propagating $y = 0.0, 1.0L_D, 2.0L_D,$ and $3.0L_D$, respectively. (a) $L = 1.0 \mu\text{m}$. The soliton forms because the Kerr nonlinearity is strong enough (due to the strong confinement effect) to balance the dispersion. (b) $L = 4.0 \mu\text{m}$. The soliton does not form because the Kerr nonlinearity is too weak.

This is in drastic contrast to conventional optical waveguides such as optical fibers, where usually the input power larger than 1.0 W is needed to obtain enough nonlinearity required for the formation of solitons [24].

To make a further confirmation on the soliton solution and check its stability, a numerical simulation is made directly from Eqs. (6) and (7). Shown in Fig. 7(a) is the result for $u = |\Omega_p/U_0|^2$ as a function of t/τ_0 for $L = 1.0 \mu\text{m}$. The initial condition is chosen as the Gaussian form $u = 1.2 \exp(-t^2/\tau_0^2)$. The curves from left to right in the figure are the waveshapes for the probe pulse propagating to $y = 0.0, 1.0L_D, 2.0L_D,$ and $3.0L_D$, respectively. We see that when propagating to $y = 1.0L_D$ the probe pulse becomes higher and sharper due to the self-phase modulation induced by the Kerr effect. Then it suffers no significant distortion during the propagation, indicating the formation of an optical soliton in the system.

To confirm the confinement effect that can increase the generating efficiency of the ultraslow optical soliton, we have made an additional simulation for the probe-pulse propagation with the same dispersion as in Fig. 7(a), but for $L = 4.0 \mu\text{m}$. The result is shown in Fig. 7(b). We see that the input pulse suffers a serious distortion during propagation. The reason is that in this case the confinement effect is weaker and hence the Kerr effect of the system is not strong enough to balance the dispersion; thus a soliton formation is not possible. However, when decreasing L to $1.0 \mu\text{m}$, the soliton forms, as shown in Fig. 7(a).

5. CONCLUSIONS

We have investigated the linear and nonlinear pulse propagations in a three-state atoms confined in a microwaveguide. Based on the MB equations we have obtained the linear dispersion relation of the probe field. We have shown that the quantum-interference effect may be greatly enhanced due to the optical confinement by the waveguide geometry. In particular, compared with the atomic gas in free space, the EIT transparency window in the present waveguide system can be much wider and deeper, the group velocity of the probe field can be much slower, and the Kerr nonlinearity of the system can be much stronger. Based on these results, we have demonstrated that ultraslow optical solitons can be more efficiently generated with an extremely low generation power. The results provided in this work may guide new experimental findings for atomic coherence and have promising applications for optical information processing and transmission.

ACKNOWLEDGMENTS

The authors thank Min Xiao for fruitful discussions. This work was supported by NSF-China under Grant Nos. 10874043 and 11174080.

REFERENCES AND NOTES

1. S. E. Harris, "Electromagnetically induced transparency," *Phys. Today* **50**(7), 36–42 (1997).
2. M. Fleischhauer, A. Imamoglu, and J. P. Marangos, "Electromagnetically induced transparency: optics in coherent media," *Rev. Mod. Phys.* **77**, 633–673 (2005).
3. J. B. Khurgin and R. S. Tucker, eds., *Slow Light: Science and Applications* (CRC, 2009).
4. A. I. Lvovsky, B. C. Sanders, and W. Tittel, "Optical quantum memory," *Nat. Photonics* **3**, 706–714 (2009).
5. M. D. Lukin and A. Imamoglu, "Nonlinear optics and quantum entanglement of ultraslow single photons," *Phys. Rev. Lett.* **84**, 1419–1422 (2000).
6. C. Ottaviani, D. Vitali, M. Artoni, F. Cataliotti, and P. Tombesi, "Polarization qubit phase gate in driven atomic media," *Phys. Rev. Lett.* **90**, 197902 (2003).
7. C. Hang, Y. Li, L. Ma, and G. Huang, "Three-way entanglement and three-qubit phase gate based on a coherent six-level atomic system," *Phys. Rev. A* **74**, 012319 (2006).
8. Y. Li and M. Xiao, "Enhancement of nondegenerate four-wave mixing based on electromagnetically induced transparency in rubidium atoms," *Opt. Lett.* **21**, 1064–1066 (1996).
9. L. Deng, M. Kozuma, E. W. Hagley, and M. G. Payne, "Opening optical four-wave mixing channels with giant enhancement using ultraslow pump waves," *Phys. Rev. Lett.* **88**, 143902 (2002).
10. Z. C. Zuo, J. Sun, X. Liu, Q. Jiang, G. S. Fu, L. A. Wu, and P. M. Fu, "Generalized n -photon resonant $2n$ -wave mixing in an $(n + 1)$ -level system with phase-conjugate geometry," *Phys. Rev. Lett.* **97**, 193904 (2006).
11. Y. Wu and L. Deng, "Ultraslow optical solitons in a cold four-state medium," *Phys. Rev. Lett.* **93**, 143904 (2004).
12. G. Huang, L. Deng, and M. G. Payne, "Dynamics of ultraslow optical solitons in a cold three-state atomic system," *Phys. Rev. E* **72**, 016617 (2005).
13. R. Santra, E. Arimondo, T. Ido, C. H. Greene, and J. Ye, "High-accuracy optical clock via three-level coherence in neutral bosonic ^{88}Sr ," *Phys. Rev. Lett.* **94**, 173002 (2005).
14. M. Wallquist, K. Hammerer, P. Rabl, M. Lukin, and P. Zoller, "Hybrid quantum devices and quantum engineering," *Phys. Scr.* **T137**, 014001 (2009).
15. S. Ghosh, J. Sharping, D. Ouzounov, and A. Gaeta, "Resonant optical interactions with molecules confined in photonic band-gap fibers," *Phys. Rev. Lett.* **94**, 093902 (2005).
16. P. S. Light, F. Benabid, F. Couny, M. Maric, and A. N. Luiten, "Electromagnetically induced transparency in Rb-filled coated hollow-core photonic crystal fiber," *Opt. Lett.* **32**, 1323–1325 (2007).
17. B. Wu, J. E. Hulbert, A. R. Hawkins, and H. Schmidt, "Planar hollow-core waveguide technology for atomic spectroscopy

- and quantum interference in alkali vapors,” *J. Lightwave Technol.* **26**, 3727–3733 (2008).
18. F. L. Kien and K. Hakuta, “Slowing down of a guided light field along a nanofiber in a cold atomic gas,” *Phys. Rev. A* **79**, 013818 (2009).
 19. D. G. Ouzounov, F. R. Ahmad, D. Müller, N. Venkataraman, M. T. Gallagher, M. G. Thomas, J. Silcox, K. W. Koch, and A. L. Gaeta, “Generation of megawatt optical solitons in hollow-core photonic band-gap fibers,” *Science* **301**, 1702–1704 (2003).
 20. M. F. Saleh, W. Chang, P. Holzer, A. Nazarkin, J. C. Travers, N. Y. Joly Philip, St. J. Russell, and F. Biancalana, “Theory of photoionization-induced blueshift of ultrashort solitons in gas-filled hollow-core photonic crystal fibers,” *Phys. Rev. Lett.* **107**, 203902 (2011).
 21. C. Hang and V. V. Konotop, “All-optical steering of light via spatial Bloch oscillations in a gas of three-level atoms,” *Phys. Rev. A* **81**, 053849 (2010).
 22. Y. Li, B. A. Malomed, M. Feng, and J. Zhou, “Arrayed and checkerboard optical waveguides controlled by the electromagnetically induced transparency,” *Phys. Rev. A* **82**, 063813 (2010).
 23. Since in our model $\omega_p \approx \omega_c$, the mode index n can be chosen according to the value of ω_p , satisfying the condition $(L/\pi c)\omega_p - 1 < n < (L/\pi c)\omega_p$.
 24. A. Hasegawa and Y. Kodama, *Solitons in Optical Communications* (Clarendon, 1995).